Fuel 88 (2009) 898–908

Contents lists available at ScienceDirect

Fuel

journal homepage: www.elsevier.com/locate/fuel

Experimental investigation of some metal oxides for chemical looping combustion in a fluidized bed reactor

M.K. Chandel [1], A. Hoteit [2], A. Delebarre *

Department of Energetics and Environmental Engineering, Ecole des Mines de Nantes, 44307 Nantes, France

ARTICLE INFO

Article history:
Received 2 May 2008
Received in revised form 2 December 2008
Accepted 9 December 2008
Available online 3 January 2009

Keywords:
Chemical looping combustion
Oxygen carriers
Fluidization

ABSTRACT

Chemical looping combustion (CLC) is the process in which metal oxides, rather than air or pure oxygen, supply the oxygen required for combustion. In this process, different gaseous fuels can be burnt with the inherent separation of CO_2. The feasibility of the CLC system depends greatly on the selection of appropriate metal oxides as oxygen carriers (OC). In this study, NiO–$NiAl_2O_4$, $Cu_{0.95}Fe_{1.05}AlO_4$, and CuO–$Cu_{0.95}Fe_{1.05}AlO_4$ were tested experimentally in a fluidized bed reactor as a function of oxidation–reduction cycles, temperature, bed inventory and superficial gas velocity. The results showed that flue gases with a CO_2 concentration as high as 97% can be obtained. The flue gases should be suitable for transport and storage after clean-up and purification. With an increase in the bed inventory or a decrease in superficial gas velocity, the flue gas characteristics improved i.e. more CO_2 and fewer secondary components or less unreacted fuel were obtained. Carbon formation could occur during the reduction phase but it decreased with an increase in temperature and inventory and could be completely avoided by mixing steam with the fuel. The reactivity of NiO/$NiAl_2O_4$ was higher than the Cu- and Fe-based oxygen carriers. Increasing the CuO fraction in the oxygen carrier led to defluidization of the bed during the reduction and oxidation phases.

1. Introduction

CO_2 is one of the major anthropogenic greenhouse gases emitted into the atmosphere. One solution is to capture CO_2 and store it permanently and safely under geological formations or deep in the sea. Chemical Looping Combustion (CLC) can be used for clean power generation as it may have a lower energy penalty due to its inherent separation of CO_2 [1] and may also be a better choice for CO_2 capture. During the last decade, considerable research has been carried out on the use of CLC for the combustion of gaseous fuels [2–9].

Chemical Looping Combustion (CLC) is an oxy-combustion in which the oxygen required for combustion is supplied by metal oxides known as oxygen carriers (OC). The CLC concept, as shown in Fig. 1, consists of two interconnected reactors known as the air and the fuel reactor. The oxygen carriers are reduced by the gaseous fuel in the fuel reactor. The reduced oxygen carriers are transferred to the air reactor where they are oxidized by air. The reactions in the air reactor are exothermic, and exothermic or endothermic in the fuel reactor depending upon the fuel and the oxygen carriers. The flue gases leaving the air reactor contain N_2 and the unreacted O_2 of air. Flue gases from the fuel reactor contain mostly CO_2, H_2O, a fraction of CO, H_2, if there is partial conversion of the fuel. However, flue gases from the fuel reactor do not contain N_2 from the air, which is the major component of flue gases from the classical combustion techniques. The partial pressure of CO_2 in the flue gases from the fuel reactor is very high. For fuels containing only C and H, pure CO_2 can be obtained after H_2O condensation.

The success of the CLC system is dependent on finding suitable oxygen carriers that have sufficiently high conversion rates in cyclic conditions of oxidation and reduction, high communition and agglomeration resistance, and are economical and environmentally friendly. The metal oxides of Ni, Cu, Fe, Co, and Mn are being tested by different researchers at different scales [10–13]. Various support materials, namely Al_2O_3, $MgAl_2O_4$, ZrO_2, and TiO_2 are used to enhance some of the desirable characteristics of oxygen carrier particles.

Ni-based oxygen carriers are considered among the most suitable for CLC. Research on these compounds has shown that YSZ, Al_2O_3, $NiAl_2O_4$, SiO_2, bentonite, and NiO/hexaaluminate can be used as a support material for NiO [14,15], while Jin et al. [16]

* Corresponding author. Address: Ecole Supérieure des Sciences et Technologies de l'Ingénieur de Nancy, 54519 Vandoeuvre-Lés-Nancy, France. Tel.: +33 (0)3 83 68 51 00; fax: +33 (0)3 83 68 50 10.
E-mail address: adelebar@esstin.uhp-nancy.fr (A. Delebarre).
[1] Present address: Climate Change Policy Partnership, Duke University, Durham, NC 27708, USA.
[2] Present address: IFP, Rond-point de l'échangeur de Solaize, BP 3, 69360 Solaize, France.

0016-2361/$ - see front matter © 2008 Elsevier Ltd. All rights reserved.
doi:10.1016/j.fuel.2008.12.006

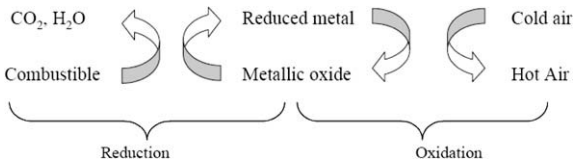

Fig. 1. Principle of chemical looping combustion.

consider that $NiAl_2O_4$ is one of the best supports. Cu- and Fe-based oxygen carriers are also good candidates. However, Cu-based oxygen carriers are limited to a lower operating temperature due to the low melting point of Cu. Fe-based OC are associated with a low oxygen-carrying capacity. Recently, a new type of material has been developed that contains oxides of copper and iron and uses Al_2O_3 as a support.

In this study, reduction–oxidation cycles under different conditions of fluidization were analyzed. The objective of this work was to study the performances of newly developed Cu–Fe-based oxygen carriers and $NiO/NiAl_2O_4$ under different experimental operating conditions: temperature, bed inventory and gas superficial velocity in the fluidized bed reactor.

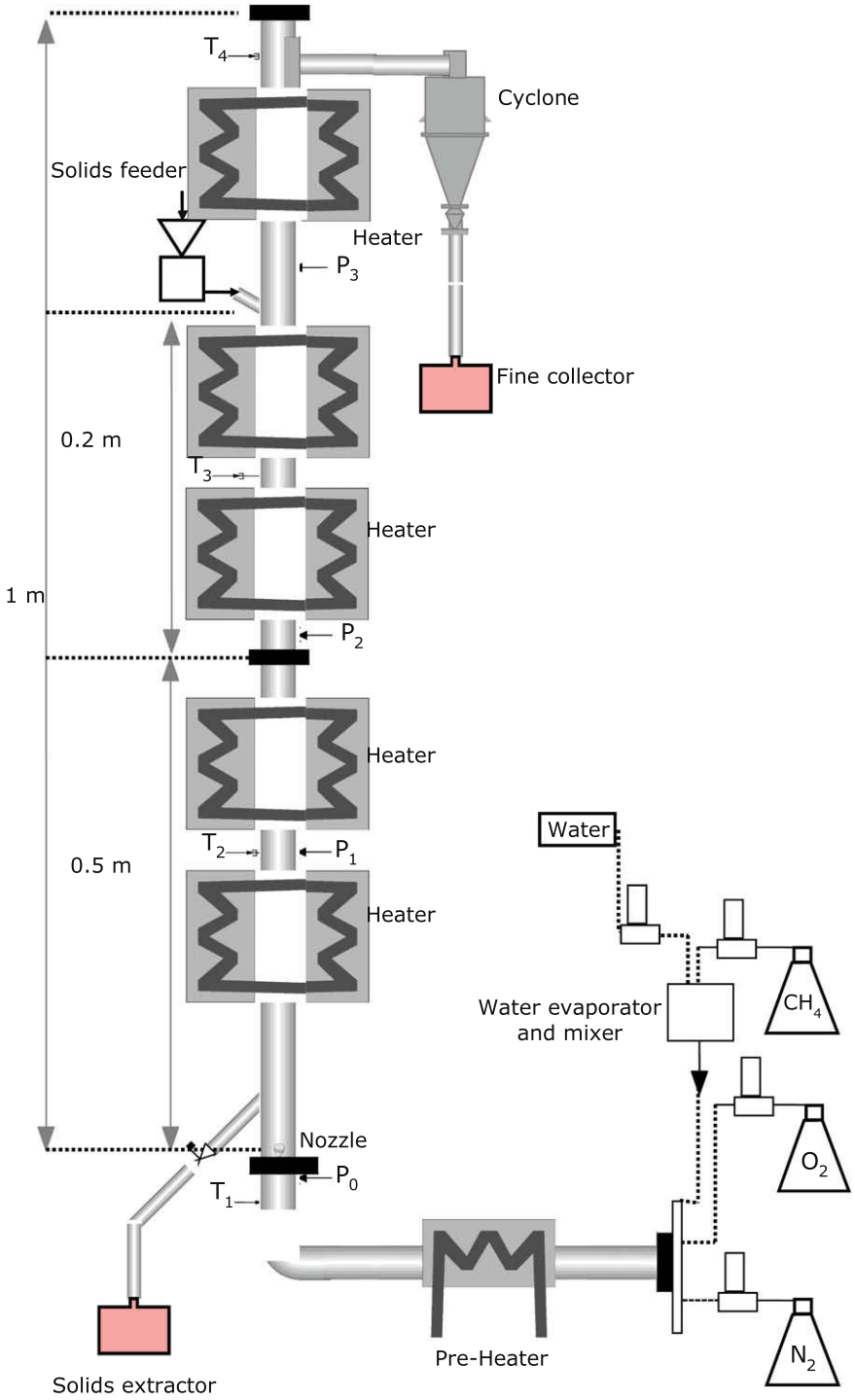

Fig. 2. Experimental equipment.

2. Materials and method

2.1. Experimental set-up

Fig. 2 presents a diagram of the pilot-scale experimental set-up. It consists of a fluidized bed reactor of 0.096 m I.D. The stainless steel reactor was designed to have three vertical columns connected in series giving a total height of 1.0 m. The reactor was equipped with access ports for temperature and pressure measurements. K-type chrome/alumel thermocouples, 0.30 m in length and 3 mm in diameter, were used to measure the temperature at three axial positions: in the bed, the pre-heater and the freeboard. The pressure difference was measured between the three sections of the reactor using pressure transducers. The reactor was pre-heated by external electrical heaters. The heating systems were regulated by three thermal regulators, each controlling the pre-heater, the bed and the freeboard.

The inflow gases were heated by a pre-heater then distributed in the bed by a nozzle. This was designed in such a way that there was a minimum pressure drop and no backflow of solids in the pre-heater. A cyclone was used to separate the elutriated solids from the flue gases.

The inflow of gases was measured by flow meters. A system of evaporation and injection of steam into the inflow gases was used, which consisted of a digital mass flow meter for liquids and a controller of evaporation and mixing. A three-way flow regulation system generated the phases of air, CH_4 with or without steam, and N_2, with adjustable durations of the different phases. Samples of outflow gas were extracted through a sintered metal filter located on top of the cyclone and pumped to a gas analyzer through the water condenser. CH_4, CO and CO_2 gas concentrations at the outlet were measured by non-dispersive infrared analysis (NDIR); O_2 concentration was measured in a paramagnetic analyzer and H_2 concentration by gas conductivity. Data were recorded using a data acquisition system connected to a personal computer running Lab view 7.0 software.

2.2. Oxygen carriers

In the present study, three types of oxygen carrier were investigated. The first was $NiO/NiAl_2O_4$ (60/40) prepared by precipitation. This Ni-based OC was manufactured by Marion Technologies (France) according to a protocol developed within the ENCAP project [17]. Its average arithmetic and harmonic diameters were 171 and 125 μm, respectively. The bulk density of the particles was 2200 kg/m^3. The BET surface area of the particles is 7 m^2/g. The maximum oxygen-carrying capacity of $NiO/NiAl_2O_4$ was measured as 14.5 wt% with thermogravimatric tests according to literature [18]. Most of the oxygen transfer capacity is accounted for by reduction of NiO to Ni (12.8%), and the remainder by the slower reduct of $NiAl_2O_4$ to Ni and Al_2O_3.

The other two oxygen carriers were made of Cu- and Fe-based metal oxides with an oxide of Al as a support material: $Cu_{0.95}Fe_{1.05}AlO_4$ and $(CuO)/(Cu_{0.95}Fe_{1.05}AlO_4)$ (23.5/76.5). The oxygen carriers were developed by IFP. These were tested with two particle size distributions each, named here CuFeAl-11 and CuFeAl-12, and CuFeAl-21 and CuFeAl-22, respectively. The batch mentioned hereafter as CuFeAl1-fine was the result of mixing equal parts of CuFeAl-11 and CuFeAl-12. The respective average arithmetic and harmonic diameters were 234 and 200 μm for CuFeAl-11; 150 and 86 μm for CuFeAl1-fine; 220 and 199 μm for CuFeAl-21 and 58 and 53 μm for CuFeAl-22. Their bulk density was around 2700 kg/m^3. The maximum oxygen-carrying capacity of $Cu_{0.95}Fe_{1.05}AlO_4$ and $(CuO)/(Cu_{0.95}Fe_{1.05}AlO_4)$(23.5/76.5) was measured as 0.095 and 0.13, respectively in a thermogravimetric tests in accordance with the literature [18].

2.3. Experimental procedure

Batches of 2.5–6 kg of oxygen carrier were used with a particle size of 0.1–0.3 mm. The inlet superficial gas velocity into the reactor was 0.05–0.15 m/s in the reduction phase and 0.15–0.3 m/s in the oxidation phase. The solid bed was pre-heated in air to the desired temperature under atmospheric pressure to ensure that the particles were fully oxidized before the reducing phase. After this phase, inert gas (N_2) was introduced for 120 s to avoid air and CH_4 mixing during the shift between the reducing and oxidizing phase. The particles were then exposed to either 100% CH_4 or a mixture of 50% CH_4 and 50% H_2O. The H_2O was introduced to study the suppressing effects of steam on carbon formation during the reduction phase.

Table 1 summarizes the different experimental conditions used. The superficial gas velocities (U_0 m/s) given are based on the gas inflow. However, superficial gas velocity would increase during

Table 1
Experimental conditions used for the reduction–oxidation cycles.

Oxygen carrier	Fuel	Temperature (°C)	Bed (kg)	Reduction time (s)	Oxidation time (s)	U_0 (m/s)	
						Reduction	Oxidation
$(NiO)_{60\%}/(NiAl_2O_4)_{40\%}$	CH_4	800,850,900	2.5	150	1100	0.15	0.3
		800	3	500	2200	0.05	0.15
		800	3	150	1100	0.15	0.3
		800	4	150	1100	0.15	0.3
		800	4	500	2200	0.05	0.15
	CH_4/H_2O (50/50)	800,850,900	2.5	240	900	0.15	0.3
CuFeAl-11	CH_4	800	3	500	1400	0.015	0.15
		800	3	500	1800	0.05	0.15
		800	3	150	1100	0.15	0.3
		850	3	400	1100	0.015	0.15
		850	3	150	1100	0.05	0.15
		850	3	150	1100	0.15	0.3
CuFeAl1-fine	CH_4	850	6	600	3400	0.015	0.06
CuFeAl-21	CH_4	800	3	150	2200	0.15	0.15
		800	3	500	2200	0.05	0.15
		800	3	900	2200	0.015	0.15
		850	3	Defluidization or partial fluidization with air or CH_4; complete fluidization with N_2			
CuFeAl-22	none	800	3	Total defluidization during heating with air			

the reduction and decrease during the oxidation due to these reactions. The conversion of oxygen carrier or the degree of oxidation (X) was defined by the Eq. (1)

$$X = \frac{m - m_{red}}{m_{ox} - m_{red}} \quad (1)$$

where m, m_{ox}, m_{red} are the actual mass of the oxygen carrier, the mass of fully oxidized and the mass of fully reduced oxygen carrier, respectively. The conversions of oxygen carrier during the reduction and oxidation phases of the cycle were evaluated by using the flue gas concentration as given in De Diego et al. [19]. The rates of reduction and oxidation were determined by Eqs. (2) and (3) respectively.

$$r_{red} = \frac{Q_{out}}{n'_{0,red}}\left(\frac{2P_{CO_2},out + P_{CO,out} + P_{H_2O,out}}{P_t ot}\right) \quad (2)$$

$$r_{ox} = \frac{2}{n'_{0,ox}}\left(Q_{in}p_{O_2},in - Q_{out}(pO_{2,out} - 1/2p_{CO,out} - p_{CO_2,out})\right) \quad (3)$$

where n_0 is the number of moles of oxygen that can be removed from fully oxidized oxygen, $n'_{0,red}$and $n'_{0,ox}$ are the moles of oxygen that are transferred during reduction and oxidation, respectively, and Q_{in}, Q_{out} are the molar flows of the incoming gas and the gas leaving the reactor respectively. Q_{in} was measured and Q_{out} was calculated from the carbon and hydrogen balance between the inflow and outflow of the gases. P_{tot} is the total pressure, $p_{j,in}$is the partial pressure of incoming gas j and $p_{j,out}$ is the partial pressure of gas j leaving the reactor and t is the time. r_{red} and r_{ox} are the conversion rates during reduction and oxidation, respectively. i is the number of the cycle. The conversion equation for the oxidation phase takes into account the formation of CO and CO_2 during the oxidation phase due to the oxidation of carbon formed in the reduction phase.

3. Results and discussion

3.1. NiO/$NiAl_2O_4$. oxygen carrier

In the case of the NiO/$NiAl_2O_4$ at 800 °C, CO_2, CO, H_2O and H_2 were formed immediately after the introduction of CH_4 into the reactor (Fig. 3). After 100 s, CH_4 reached near to complete conversion, whilst a certain amount of CO and H_2, which is associated with the thermodynamic limitation of NiO to convert CH_4 fully to CO_2 and H_2O, was observed. After 100 s, the concentration of CO_2 decreased whereas the concentrations of CO and H_2 increased, indicating that the reducing process was mainly selective towards the formation of CO and H_2. The change in product selectivity during the reducing step was probably associated with changes in the degree of oxidation of the carrier. At the beginning, the fully oxidized oxygen carrier favored the total oxidation of CH_4. As the OC was reduced, the selectivity of product formation changed from CO_2 and H_2O to CO and H_2, possibly assisted by the occurrence of the CH_4 reforming reaction, catalyzed by reduced Ni active sites. During the oxidation phase, after O_2 was introduced into the reactor, a peak of CO_2 immediately appeared in the reactor outlet gases. This was due to the carbon deposits in the preceding reduction phase. In the beginning of oxidation phase, there was no oxygen in the product gases, indicating the complete consumption of O_2 in the reaction, and then increased to 21%. The product concentra-

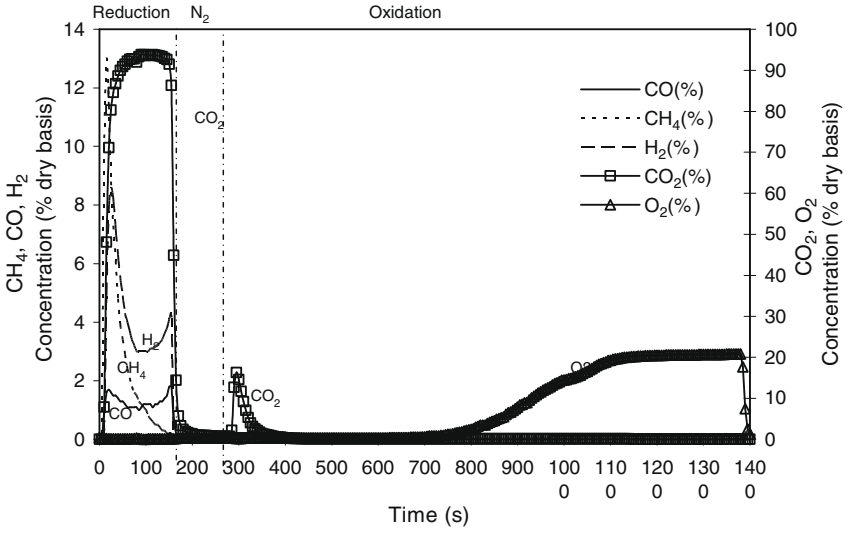

Fig. 3. Outlet gas concentrations during a reduction–oxidation cycle at 800 °C with NiO/$NiAl_2O_4$ and a bed inventory of 2.5 kg.

Table 2
Outlet gas composition (% dry basis) for the reduction phase with different bed masses and superficial gas velocities at a bed temperature of 800 °C for the NiO/$NiAl_2O_4$ oxygen carrier.

Temperature (°C)	800						850		900	
Bed mass (kg)	4		3		2.5		2.5		2.5	
Reduction phase	CH_4		CH_4		CH_4	CH_4/H_2O (50/50)	CH_4	CH_4/H_2O (50/50)	CH_4	CH_4/H_2O (50/50)
CH_4 flow rate (Nm^3/h)	0.1	1.0	0.1	1.0	1.0	0.5	1.0	0.5	1.0	0.5
Superficial gas velocity (m/s)	0.05	0.15	0.05	0.15	0.15	0.15	0.15	0.15	0.15	0.15
Number of cycles	4	10	2	2	10	5	10	5	10	5
CO_2 (%)	97	95	96	94	94	90.3	93.9	92.5	93.6	93.3
CH_4 (%	0.2	1.5	0.3	1.5	1.2	0.6	0.8	0.5	0.4	0.5
CO (%)	0.6	0.8	0.9	1	0.8	1.3	1.1	1.3	1.5	1.2
H_2 (%)	1.2	2.2	1.9	2.7	3.0	4.6	3.1	3.8	3.4	3.5

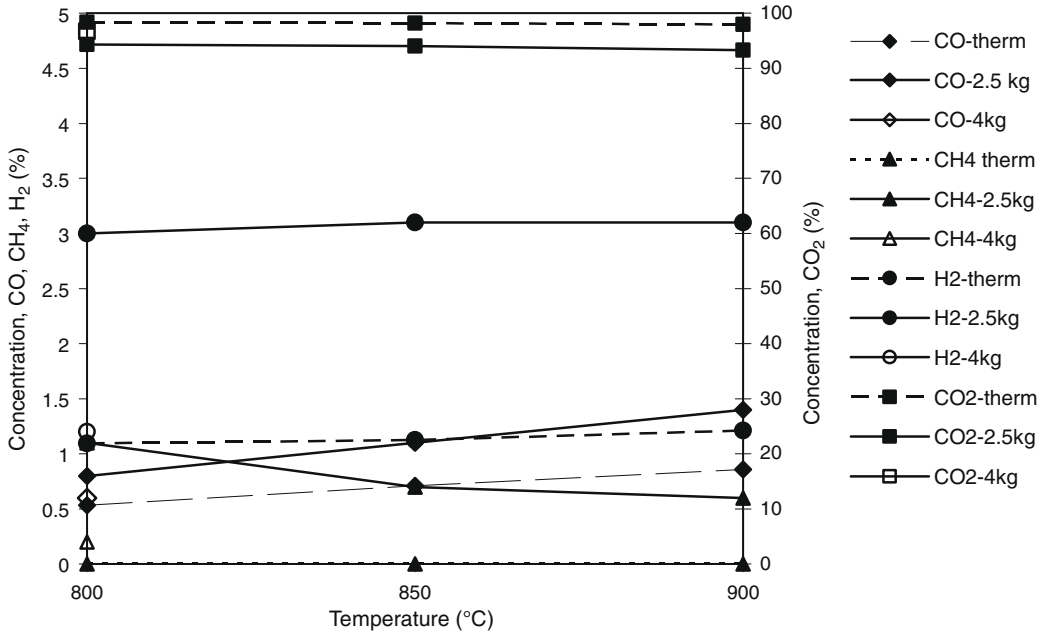

Fig. 4. Comparison of the thermodynamic equilibrium composition and the actual flue gas composition obtained at different temperatures for $NiO/NiAl_2O_4$ with bed inventories of 2.5 and 4 kg.

tion profiles at the outlet stream as a function of the reaction time were not affected by the number of cycles indicating the good chemical stability of the Ni-based oxygen carrier.

Table 2 shows the flue gas composition for the reduction phase for different bed mass and superficial gas velocities. For 0.15 m/s and 4 kg of OC, the maximum outlet CO_2 concentration was

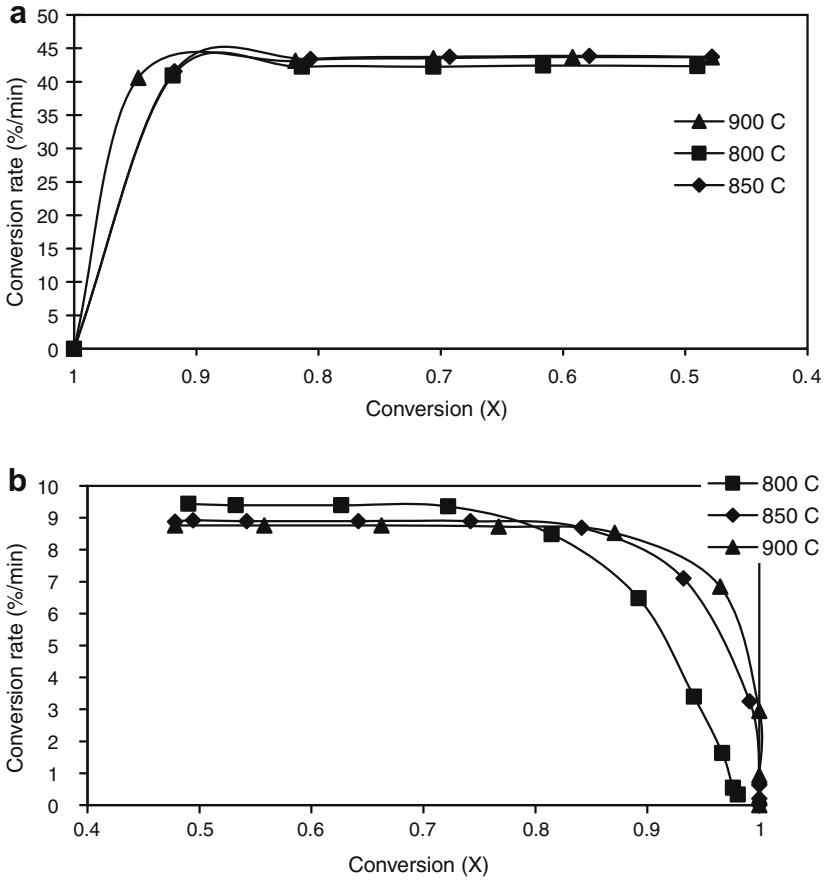

Fig. 5. Variations in conversion rate of $NiO/NiAl_2O_4$ with the degree of conversion at different temperatures with 2.5 kg of bed in (a) the reduction phase (b) the oxidation phase.

94.7% and unreacted CH_4 was 1.5%. CO and H_2 outlet concentrations were 0.8% and 2.2%, respectively. For the same bed mass (4 kg), the decrease in superficial gas velocity improved flue gas characteristics i.e. the CO and H_2 decreased. Methane conversion was higher at a lower velocity: 99.8% (0.05 m/s) and 98.5% (0.15 m/s). For the same superficial gas velocity, an increase in the bed mass decreased the CO and H_2 concentration in the outlet gases, whilst there was also a slight increase in CO_2 concentration, as if the increase in the particle–gases contact time improved the methane conversion both quantitatively and qualitatively. For the same inlet CH_4 velocity, the increase in the bed mass did not affect the reactivity of the oxygen carrier. The variations in bed inventory and flow rate are the parameters controlling the contact time between gas and solids. With an increase in the bed inventory, this contact time increased and hence CH_4 was better oxidized. For the same reasons, a better oxidation of CH_4 occurred at a lower superficial gas velocity.

Fig. 4 shows the experimental flue gas composition for 2.5 and 4 kg and the thermodynamic equilibrium compositions as a function of temperature. For 2.5 kg of NiO oxygen carrier, there was no major variation in the CO_2 outlet concentration as a function of temperature (94%). The H_2 outlet concentration remained equal to nearly 3% for all experimental temperatures. The CO outlet concentration increased from 0.8–1.4% when the temperature was increased from 800 °C to 900 °C. CH_4 concentration in the flue gases decreased steadily with time and approached 0.2% towards the end of the reduction phase. The outlet concentration was far from the equilibrium composition. For CO_2, the concentration of the equilibrium composition was 98% while the experimental values correspond to 94%. At 800 °C and with 4 kg as a bed inventory, the outlet product composition was very close to the thermodynamic equilibrium composition.

Fig. 5(a) and (b) shows the conversion rate of $NiO/NiAl_2O_4$ for reduction and oxidation, respectively. The degree of conversion varied from 1.0 to 0.46 during reduction and 0.46–1 during oxidation. The conversion rate during reduction was constant after the initial increase, which was due to the phase change. The conversion rates were limited by the inflow of reacting gases. The maximum conversion rate at 900 °C for reduction and oxidation was 43.8%/min and 9.4%/min, respectively. Cho et al. [10] demonstrated a conversion rate of 50%/min in the reduction phase and 4.2% in the oxidation phase for the same type of oxygen carriers at 950 °C. Fig. 5(b) shows that the conversion rate of the carrier during oxidation was constant up to a degree of conversion of 0.8 and then decreased sharply as the degree of conversion increased from 0.8 to 1.0. With the decrease in the temperature, the conversion rate decreased. This shows that the conversion rate at high values of X (i.e. from 0.8 to 1.0) may not be sufficient for the commercial chemical looping combustion application. Moreover, lower values of X in a fuel reactor would lead to partially oxidized outlet gases.

Fig. 6 shows the flue gas composition (% dry basis) at 850 °C. In the initial phase of reduction (0–25 s), the concentrations of CO, CH_4, and H_2 were higher and, as the phase stabilized, the concentration of these gases decreased and became steady. H_2 concentration was higher with steam than without. The same trend can be seen with CO.

3.2. Carbon formation

As mentioned earlier, there was carbon formation during the reduction of CH_4 as seen by the peak of CO_2 at the beginning of the oxidation phase in Fig. 6(a). The carbon deposited during the reduction phase was oxidized to CO_2 during the oxidation phase. Table 3 shows the average carbon formation at different tempera-

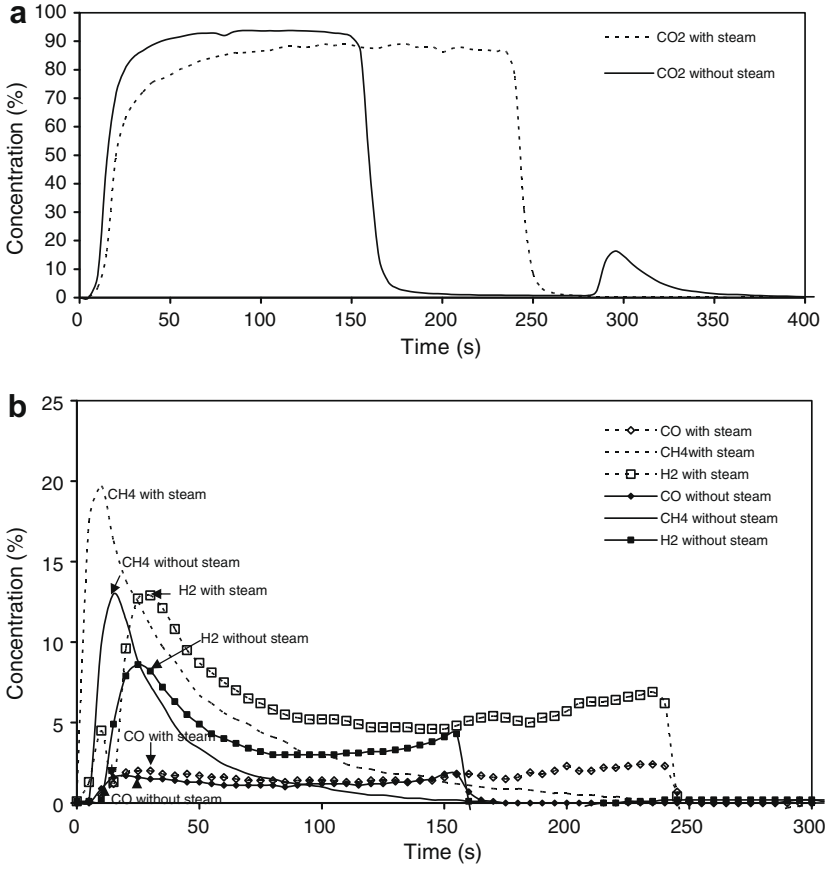

Fig. 6. Comparison of flue gas concentration (% dry basis) for $NiO/NiAl_2O_4$ at 2.5 kg of bed mass without and with 50 % steam at 850 °C: (a) CO_2 (b) CO, CH_4 and H_2.

Table 3
Carbon formation during the reduction stage for $NiO/NiAl_2O_4$.

Temperature (°C)	C/C_{total} (%)			
	Without steam	With steam	Inventory (kg)	U_0 (m/s)
800	9.25	0.32	2.5	0.15
850	8.79	0.27	2.5	0.15
900	4.25	0.29	2.5	0.15
800	3.01	–	3	0.05
800	1.64	–	3	0.15
800	2.96	–	4	0.05
800	1.67	–	4	0.15

tures with and without steam, given as a percentage of the total flow of carbon during the reduction phase. The carbon deposition decreased with increasing temperature. Thus, increasing the temperature from 800 °C to 900 °C led to a decrease in carbon formation from 9.25% to 4.25%. This phenomenon may be due to the oxidation of carbon at a higher temperature. The addition of steam to the inflow of CH_4 completely prevented the carbon formation. This may be due to the carbon deposit being reduced by carbon gasification which produces CO and H_2. Table 3 also shows that an inventory increase from 2.5 to 3.0 kg led to a carbon formation decrease from 9.26% to 1.64%. However, a further increase in the bed inventory to 4.0 kg did not affect carbon formation. Carbon formation also decreased with the increase in superficial gas velocity during reduction.

Cho et al. [20] mentioned two possible mechanisms of carbon formation during reduction: methane decomposition and the Boudouard reaction (Eqs. (4) and (5)). Kinetically, both of these are slow in the absence of a catalyst. However, metals such as Ni and Fe could act as a catalyst. For the temperature range used during the present experiments, methane decomposition is favored over the Boudouard reaction. Carbon deposition may have started when there was sufficient Ni present, i.e. towards the end of the reduction phase. These results imply that there is a competition between reaction of CH_4 with NiO and cracking of CH_4 in the presence of Ni metal acting as a catalyst. The CH_4 cracking at high temperature in the presence of Ni metal could have lead to high concentrations of CO and H_2. The NiO reaction with CH_4 led to the generation of Ni, which could have acted as a catalyst for CH_4 decomposition and hence carbon formation on the outer surface of the particles. Carbon formation may have further blocked the reaction between the oxygen in the inner core of

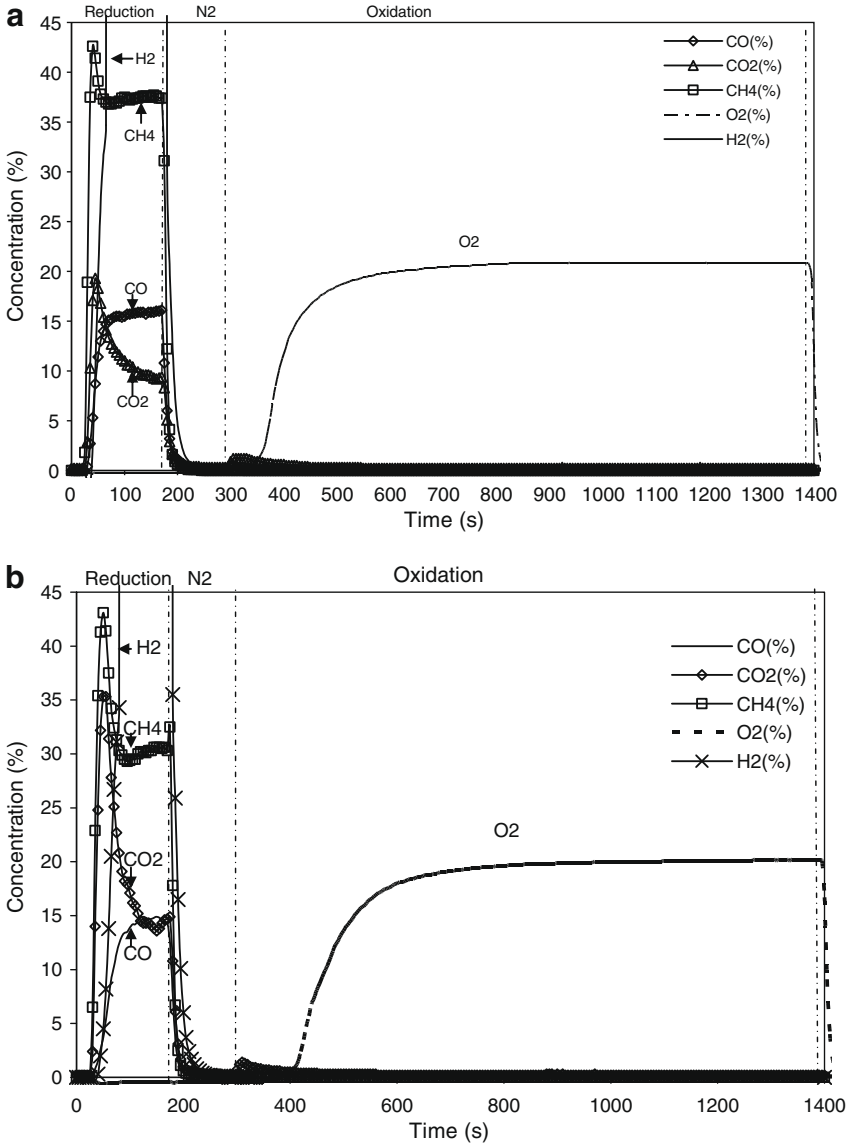

Fig. 7. Outlet gas concentrations (% dry basis) as a function of time during one cycle with 3 kg of CuFeAl-11 and 1.0 Nm^3/h of CH_4 at (a) 800 °C and (b) 850 °C.

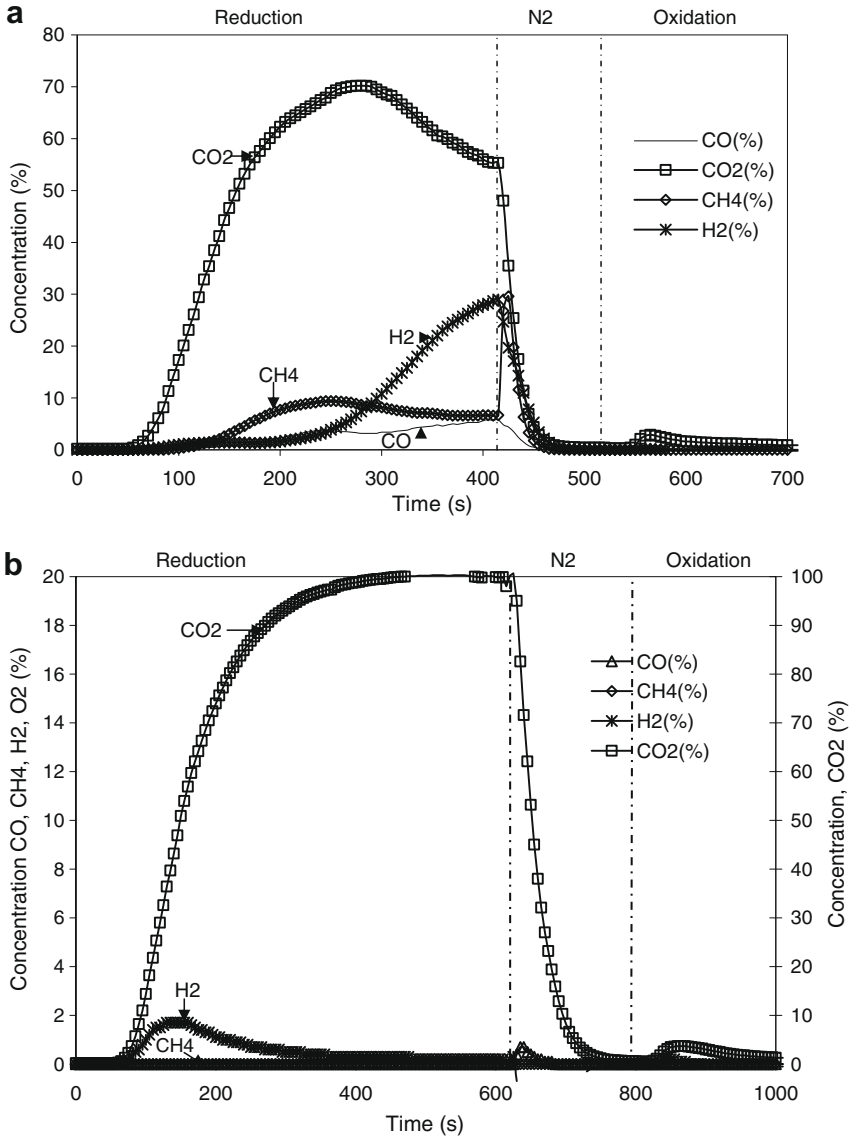

Fig. 8. Outlet gas concentrations (% dry basis) as a function of time for the reducing phase at 0.1 Nm^3/h of CH_4 at 850 °C with (a) CuFeAl-11 bed mass of 3 kg and (b) CuFeAl1-fine bed mass of 6 kg.

the particles and the gases. That could explain why, even in the presence of sufficient NiO, a significant quantity of CO and H_2 was formed.

$$CH_4 \rightarrow C + 2H_2 \text{ (Methane decomposition)} \quad (4)$$

$$2CO \rightarrow C + CO_2 \text{ (Boudouard reaction)} \quad (5)$$

The decrease in carbon formation with the addition of steam to methane may be associated with steam reforming and the shift reaction as described by Jin et al. [15].

$$CH_4 + H_2O \rightarrow CO + 3H_2 \text{ (Stream reforming)} \quad (6)$$

$$CO + H_2O \rightarrow CO_2 + H_2 \text{ (Shift reaction)} \quad (7)$$

Table 4
Outlet gas composition (% dry basis) for the reduction phase at different bed masses, superficial gas velocities and temperatures for three CuFeAl oxygen carriers.

Oxygen carrier	CuFeAl-11						CuFeAl1-fine	CuFeAl-21		
Temperature (°C)	800			850			850	800		
Bed mass (kg)	3			3			6	3		
CH_4 flow rate (Nm^3/h)	0.1	0.3	1.0	0.1	0.15	0.3	0.1	0.1	0.3	1.0
Superficial gas velocity (m/s)	0.015	0.045	0.15	0.015	0.022	0.045	0.015	0.015	0.045	0.15
Number of cycles	2	2	2	2	2	2	4	2	2	2
CO_2 (%)	42.6	16.6	9.7	67.8	62	48.6	99.9	94.1	74.7	51.6
CH_4 (%	8.7	22.5	37.4	6.3	11.6	16.8	0	1.8	22.8	46.5
CO (%)	5.6	15.2	15.9	3.0	7.1	10.4	0	0.1	0.6	0.3
H_2 (%)	28.4	>30	>30	26	21	>30	0	0.1	3.1	2.9

Another possible reason for the smaller carbon presence is that steam injection might have gasified the carbon as in Eq. (8)

$$C + H_2O \rightarrow CO + H_2 \quad (8)$$

The reaction between steam and coke can produce CO and H_2 without the intervention of NiO or Ni in the reaction. In the presence of steam, the steam reforming of coke can take place as in equation (8). The products H_2 and CO from the above reactions

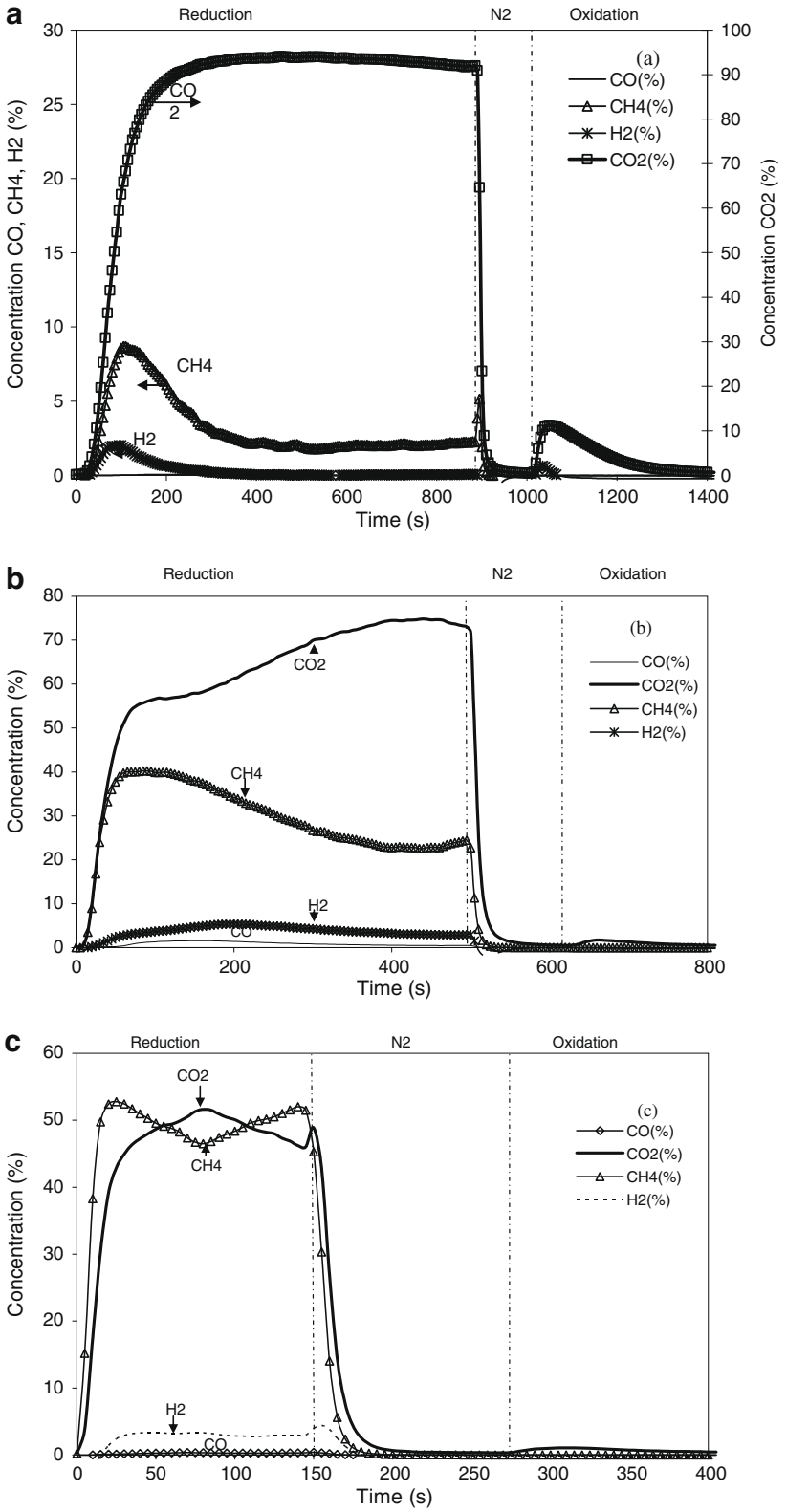

Fig. 9. Outlet gas concentrations (% dry basis) as a function of time for the reducing phase at 800 °C with CuFeAl-21 and 3 kg of bed mass at (a) 0.1 Nm^3/h (b) 0.3 Nm^3/h (c) 1.0 Nm^3/h of CH_4.

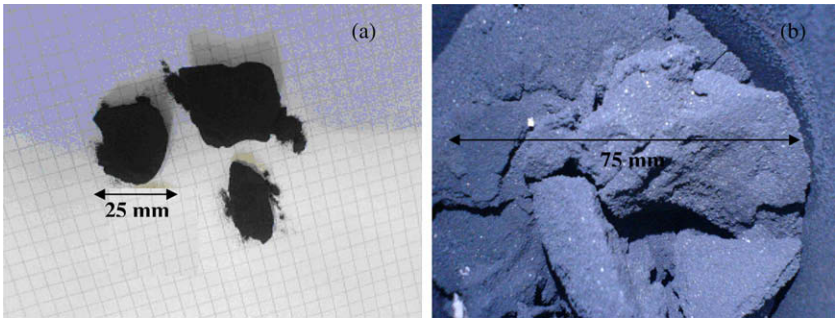

Fig. 10. CuFeAl oxygen carrier agglomeration at (a) 800 °C for CuFeAl-22 (b) 850 °C for CuFeAl-21; complete bed agglomeration.

might have been further oxidized by NiO to give CO_2 and H_2O. The shift reaction also explains the higher H_2 concentration during the reduction with the steam–CH_4 mixture. The addition of steam led to CO and H_2 as intermediate products and some of these gases may not have reacted further with NiO and hence their concentration in the outlet increased.

3.3. CuFeAl oxygen carriers

Fig. 7 (a) shows the outlet gas concentrations, % dry basis, as a function of time during the reducing phase with 3 kg of CuFeAl-11 and 0.15 m/s of CH_4 at 800 °C. Unreacted CH_4 was detected along with CO_2 which decreased and stabilized at 37.5% towards the end of the phase. There was also a fraction of CO and H_2 that started to increase when the peak of CO_2 decreased towards the end of the phase. The H_2 concentration sometimes exceeded the maximum measurement capacity of the analyzer (30%) and CO concentration was stabilized at 16%.

In the start of the oxidation phase, all the incoming oxygen reacted with reduced OC resulting in no oxygen in the outflow. Then the oxygen increased rapidly to 21%. A small peak of CO_2 (less than 1.5%) was observed at the beginning of the oxidation phase indicating a small amount of carbon deposition in the bed during preceding reduction phase. With the increase in temperature to 850 °C (Fig. 7 (b)), the reactivity of the oxygen carrier increased marginally. The outflow gases were better oxidized by CuFeAl-11 when the inlet flow of CH_4 was decreased to 0.015 m/s of CH_4 (Fig. 8 (a)).

For the CuFeAl1-fine OC at 850 °C, 0.015 m/s of CH_4 and 6 kg of oxygen carrier, a complete conversion of CH_4 was obtained (Fig. 8 (b)). The CO_2 outlet concentration approached 100% which confirms the complete reduction of CH_4 to CO_2 and H_2O. Table 4 shows the variations in an outlet gas composition for the reduction phase in different operating conditions for CuFeAl. As can be seen, the decrease in the superficial gas velocity led to a better reduction of CH_4, which was related to an increase in the residence time with the superficial gas velocity decrease. Thus the increase in contact time between the CH_4 and OC, by either reducing the superficial gas velocity or increasing the bed mass, led to an improvement in the reduction of CH_4. The increase in temperature also increased the conversion of CH_4.

Fig. 9(a, b and c) shows the outlet gas concentrations (% dry basis) as a function of time for the reducing phase with 3 kg of CuFeAl-21 and different flow rates of CH4 at 800 °C. From Table 4, it is clear that the reduction characteristics of CuFeAl-21 were similar to those of CuFeAl-11 (i.e. a decrease in superficial velocity led to an enhanced reduction of CH_4). In comparison with CuFeAl-11, the reduction characteristics of CuFeAl-21 were better for the same flow rate of CH_4. The improved reaction characteristics of CuFeAl-21 may be attributed to the presence of free CuO.

However, at 850 °C, defluidization of the bed occurred during the reduction and oxidation phases with CuFeAl-21. During the neutral phase of N_2, the bed was fluidizing normally but the switch from N_2 to air provoked defluidization, which was detected by the sudden changes in the bed pressure drop, as well as by the bed extraction at the end of the experiments. Agglomerates were observed even though they were breakable with a small force. Fig. 10 (a & b) shows the agglomeration at 800 °C for CuFeAl-22 and at 850 °C for CuFeAl-21. For CuFeAl-22, the agglomeration appeared at the beginning of the initial heating and was detected by a sharp decrease in the bed pressure. De Diego et al. [19] considered that all the OC with CuO contents greater than 20 wt% agglomerated regardless of the preparation method, the number of impregnations, or the calcination temperature used in their manufacture. The selection of a suitable composition of Cu and Fe should avoid the problem of defluidization, taking into account the operating temperature. In contrast to CuFeAl, defluidization was never observed for the Ni-based OC.

The results obtained for all oxygen carriers demonstrate the feasibility of their advantages when scaling up their use in an industrial application. The Ni-based carrier allows reducing the size of reactors and bed inventories, whilst it remains an expensive and toxic product. The FeCu-based oxygen carrier is cheaper and not toxic but leads to much bigger installations and inventories. Calculations for an industrial power plant based on the respective performances of these two carriers shows tremendous differences in reactor and bed sizing whatever the gaseous fuel is [7]. The oxygen carrier that may defluidize due to agglomeration have to be avoided in order to keep a steady and safe operation of an installation, without requiring a temperature control too sophisticated.

4. Conclusions

Ni- and CuFe-based oxygen carriers for chemical looping combustion were investigated in a batch fluidized bed reactor for the cycles of reduction and oxidation with methane and air respectively at different temperatures, flow rates, and bed inventories. It was found that a CO_2 yield as high as 97% could be achieved for both types of oxygen carrier. With an increase in bed inventory or a decrease in superficial gas velocity, flue gas characteristics improved i.e. there was more CO_2 and fewer secondary components or less unreacted fuel.

The maximum conversion rate at 900 °C for NiO/$NiAl_2O_4$ reduction and oxidation phases was 43.8%/min and 9.4%/min respectively. A lower temperature decreased the oxidation conversion rate when the reaction was not controlled by the inflow of oxygen. There was carbon formation during the reduction phase but this could be completely avoided by mixing steam with the fuel. An increase in superficial gas velocity and temperature decreased the carbon formation.

With CuFeAl-based oxygen carrier, the reduction rate of the oxygen carriers was lower than NiO/$NiAl_2O_4$. An increasing percentage of CuO in the oxygen carrier led to an increase in reactivity.

However, with a high percentage of CuO, there were signs of defluidization at 850 °C. Defluidization occurred even at low temperatures, especially when the particle size distribution was smaller. There were no signs of defluidization for $NiO/NiAl_2O_4$. A decrease in the superficial gas velocity led to a better reduction of CH_4 as did an increase in the bed inventory. The reactivity difference between Ni and CuFeAl oxygen carrier will change the reactor and bed dimensions of the reactors of the application. For the same fuel conversion, more CuFeAl would be required compared to Ni-based oxygen carrier. As Ni-based oxygen carrier is costlier than CuFeAl oxygen carrier, there will be a trade-off in the cost of the oxygen carrier versus the cost of the reactors. Moreover, the constraints imposed by the "purity" of CO_2 to be captured may also be used as selection criteria for the oxygen carrier.

Further work to be done in Ecole des Mines de Nantes will be devoted to a more precise and complete modeling of the scale-up improved by integration of a more complete set of chemical equations, the kinetics evaluations of their characteristics. Furthermore, empirical evaluation of the ageing of the carriers regarding their particle size distribution and the production rate of fine particles during succeeding phase of reduction and oxidation, as well as the analysis of the ageing of their capacity and rates during their use.

Acknowledgments

The authors are grateful to the French National Research Agency for its financial support. Oxygen carriers were synthesized by Marion Technologies and IFP. We also thank M. Lambert (IFP) for fruitful discussions. Munish Chandel and Arnaud Delebarre also thank the "Region Pays de la Loire", France, for its financial support to Munish Chandel during his one-year stay in the Energetics and Environmental Engineering Department of the Ecole des Mines de Nantes.

References

[1] Brandvoll Ø, Bolland O. Inherent CO_2capture using chemical looping combustion in a natural gas fired power cycle. J Eng Gas Turb Power 2004;26:316–21.
[2] Ishida M, Jin H. A novel chemical-looping combustor without NO_x formation. Ind Eng Chem Res 1996;35:2469–72.
[3] Ishida M, Jin H, Okamoto T. Kinetic behavior of solid particle in chemical-looping combustion: suppressing carbon deposition in reduction. Energ Fuel 1998;12:223–9.
[4] Ryu HJ, Lim NY, Bae DH, Jin GT. Carbon deposition characteristics and regenerative ability of oxygen carrier particles for chemical looping combustion. Korea Chem Eng 2003;2:157–62.
[5] Mattisson T, Johansson M, Lyngfelt A. Multicycle reduction and oxidation of different types of iron oxide particles-application to chemical-looping combustion. Energ Fuel 2004;18(3):628–37.
[6] Garcia-Labiano F, Adanez J, de Diego L, Gayan P, Abad A. Effect of pressure on the behavior of copper-, iron-, and nickel-based oxygen carriers for chemical-looping combustion. Energ Fuel 2006;20:26–33.
[7] Chandel MK, Hoteit A, Delebarre A. Clean power generation from syngas and biogas using chemical looping combustion: simulation and comparison. In: Third european combustion meeting. ECM 2007, Crete, Greece: Mediterranean Agronomic Institute of Chania; 2007. [Paper no. 12–13].
[8] de Diego LF, Garcia-Labiano F, Adanez J, Gayan P, Abad A, Corbella BM, et al. Development of Cu-based oxygen carriers for chemical-looping combustion. Fuel 2004;83:1749–57.
[9] Lyngfelt A, Leckner B, Mattisson T. A fluidized-bed combustion process with inherent CO_2 separation; application of chemical-looping combustion. Chem Eng Sci 2001;56:3101–13.
[10] Cho P, Mattisson T, Lyngfelt A. Comparison of iron-, nickel-, copper and manganese-based oxygen carriers for chemical-looping combustion. Fuel 2004;83:1215–25.
[11] Abad A, Adanez J, Garcia-Labiano F, de Diego LF, Gayan P, Celaya J. Mapping of the range of operational conditions for Cu-, Fe-, and Ni-based oxygen carriers in chemical-looping combustion. Chem Eng Sci 2007;62:533–49.
[12] Zafar Q, Mattisson T, Gevert B. Redox investigation of some oxides of transition-state metals Ni, Cu, Fe, and Mn Supported on SiO_2 and $MgAl_2O_4$. Energ Fuel 2006;20(1):34–44.
[13] Johansson E, Mattisson T, Lyngfelt A. Investigation of $Mn_3\ O_4$ with stabilized ZrO_2 for chemical-looping combustion. Chem Eng Res Des 2006;84(A9): 807–18.
[14] Song KS, Seo YS, Yoon HK, Cho SJ. Characteristics of the NiO/Hexaaluminate for chemical looping combustion. Korean J Chem Eng 2003;20(3):471–5.
[15] Adanez J, de Diego LF, Garcıa-Labiano F, Gayan P, Abad A. Selection of oxygen carriers for chemical-looping combustion. Energ Fuel 2004;18(2): 371–7.
[16] Jin H, Okamoto T, Ishida M. Development of a novel chemical-looping combustion: synthesis of a solid looping material of $NiO/NiAl_2O_4$. Ind Eng Chem Res 1999;38:126–32.
[17] Mattisson T, Leion H, Lyngfelt A. Chemical-looping with oxygen uncoupling using CuO/ZrO_2 with petroleum coke. Fuel 2008;88(4):683–90.
[18] Ishida M, Yamamoto M, Ohba T. Experimental results of chemical-looping combustion with $NiO/NiAl_2O_4$ particle circulation at 1200 C. Energ Convers Manage 2002;43:1469–78.
[19] de Diego LF, Gayan P, Garcia-Labiano F, Celaya J, Abad A, Adanez J. Impregnated CuO/Al_2O_3 oxygen carriers for chemical-looping combustion: avoiding fluidized bed agglomeration. Energ Fuel 2005;19:1850–6.
[20] Cho P, Mattisson T, Lyngfelt A. Carbon formation on nickel and iron oxide-containing oxygen carriers for chemical-looping combustion. Ind Eng Chem Res 2005;44(4):668–76.